

# Spatial distribution and network morphology of epicardial, endocardial, interstitial, and Purkinje cell-associated elastin fibers in porcine left ventricle

Xiaodan Shi <sup>a</sup>, Song Zhang <sup>b</sup>, Yue Liu <sup>c</sup>, Bryn Brazile <sup>b</sup>, Jim Cooley <sup>b</sup>, J. Ryan Butler <sup>b</sup>, Sara R. McMahan <sup>a</sup>, Karla L. Perez <sup>a</sup>, Jiazhu Xu <sup>a</sup>, Timothy Eastep <sup>a</sup>, Kytai T. Nguyen <sup>a</sup>, Pietro Bajona <sup>e,f</sup>, Matthias Peltz <sup>e</sup>, Huajian Gao <sup>c,d</sup>, Yi Hong <sup>a,\*\*</sup>, Jun Liao <sup>a,\*</sup>

<sup>a</sup> Department of Bioengineering, University of Texas at Arlington, Arlington, TX, 76010, USA

<sup>b</sup> College of Engineering and College of Veterinary Medicine, Mississippi State University, Mississippi State, MS, 39762, USA

<sup>c</sup> School of Engineering, Brown University, Providence, RI, 02912, USA

<sup>d</sup> College of Engineering, Nanyang Technical University, 308232, Singapore

<sup>e</sup> Department of Cardiovascular and Thoracic Surgery, University of Texas Southwestern Medical Center, Dallas, TX, 75390, USA

<sup>f</sup> Allegheny Health Network-Drexel University College of Medicine, Pittsburgh, PA, 15212, USA

## ARTICLE INFO

### Keywords:

Heart ECM  
Epicardial elastin  
Endocardial elastin  
Interstitial elastin  
Purkinje-cell associated elastin

## ABSTRACT

Cardiac extracellular matrices (ECM) play crucial functional roles in cardiac biomechanics. Previous studies have mainly focused on collagen, the major structural ECM in heart wall. The role of elastin in cardiac mechanics, however, is poorly understood. In this study, we investigated the spatial distribution and microstructural morphologies of cardiac elastin in porcine left ventricles. We demonstrated that the epicardial elastin network had location- and depth-dependency, and the overall epicardial elastin fiber mapping showed certain correlation with the helical heart muscle fiber architecture. When compared to the epicardial layer, the endocardial layer was thicker and has a higher elastin-collagen ratio and a denser elastin fiber network; moreover, the endocardial elastin fibers were finer and more wavy than the epicardial elastin fibers, all suggesting various interface mechanics. The myocardial interstitial elastin fibers co-exist with the perimysial collagen to bind the cardiomyocyte bundles; some of the interstitial elastin fibers showed a locally aligned, hinge-like structure to connect the adjacent cardiomyocyte bundles. This collagen-elastin combination reflects an optimal design in which the collagen provides mechanical strength and elastin fibers facilitate recoiling during systole. Moreover, cardiac elastin fibers, along with collagen network, closely associated with the Purkinje cells, indicating that this ECM association could be essential in organizing cardiac Purkinje cells into “fibrous” and “branching” morphologies and serving as a protective feature when Purkinje fibers experience large deformations in vivo. In short, our observations provide a structural basis for future in-depth biomechanical investigations and biomimicking of this long-overlooked cardiac ECM component.

## 1. Introduction

Cardiovascular disease (CVD) is the leading cause of death globally, accounting for approximately 17.8 million deaths in 2017 and is an expensive healthcare burden [1]. CVD Statistics in the US further shows that coronary heart disease was responsible for 365,914 deaths (~13% of deaths) in 2017 [1]. After coronary artery blockage, the downstream

cardiomyocytes die and lead to myocardial infarction (MI) [2–4], subsequently resulting in scar tissue formation, left ventricular wall thinning and dilatation, loss of cardiac function, and eventually fatal heart failure [5–12]. In order to prevent the adverse remodeling of the ventricular wall, current treatments include fibrinolytic therapies and surgical interventions such as coronary artery bypass grafting and angioplasty, for a timely revascularization [12,13]. However, those

Peer review under responsibility of KeAi Communications Co., Ltd.

\* Corresponding author. Department of Bioengineering The University of Texas at Arlington, Arlington, Texas, 76010, USA.

\*\* Corresponding author. Department of Bioengineering The University of Texas at Arlington, Arlington, Texas, 76010, USA.

E-mail addresses: [yihong@uta.edu](mailto:yihong@uta.edu) (Y. Hong), [jun.liao@uta.edu](mailto:jun.liao@uta.edu) (J. Liao).

<https://doi.org/10.1016/j.bioactmat.2022.04.019>

Received 2 December 2021; Received in revised form 7 April 2022; Accepted 18 April 2022

Available online 26 April 2022

2452-199X/© 2022 The Authors. Publishing services by Elsevier B.V. on behalf of KeAi Communications Co. Ltd. This is an open access article under the CC BY-NC-ND license (<http://creativecommons.org/licenses/by-nc-nd/4.0/>).

treatments cannot effectively replace the necrotic scar tissues when revascularization is delayed [14–16]. New MI therapeutic efforts include stem cell therapy and grafting of tissue engineered cardiac constructs. These innovative approaches still face great challenges in achieving cell retention, proper cell differentiation and cell-extracellular matrix (ECM) interaction, efficient vascularization, and matched mechanical properties [17–20]. To facilitate the success of new therapeutic efforts, we need a better understanding of not only the cellular behaviors in cardiac tissues, but also the properties of cardiac ECM.

In the human body, tissues can never achieve their mechanical functions only via cells. The cells, either one type or several types, must be organized into a 3D structure, and this 3D organization is realized by interweaving each individual cell with structural ECMs. In the heart, cardiac ECM is essential in mediating tissue structure and its functions, including structural support for cells, tethering and force transferring among cardiomyocytes, and prevention of excessive myocardial fiber stretch [21–25]. Similar to other functional tissues, collagen, elastin, and proteoglycans are three major structural ECM components in the heart [22]. Previous research in cardiac ECMs has mainly focused on collagen (types I and III) due to its crucial role in organizing the multilayered helical myocardial fibers, facilitating force transmission among muscle fibers, and remodeling in response to physiological and pathophysiological alterations [22–24].

Despite a few studies hinted that elastin might have an important role in cardiac mechanics and function [1,22,26], its structural and mechanical function in the heart are still poorly understood when compared to the knowledge of elastin in other soft tissues, such as blood vessels, heart valves, lung alveoli, skin, and ligaments. To date, the studies of cardiac elastin have mainly focused on physiological and pathological aspects [27–29]. For example, the mutation of elastin gene has been found to cause deficiency or abnormal deposition of elastin and eventually result in Williams syndrome (WS), that includes structural lesions such as ventricular septal defects and ventricular hypertrophy [27–29]. Another focus of elastin study is the vascular elastin in the coronary blood vessels. The vascular elastin was found to contribute significantly to the composition and stiffness of coronary blood vessels in response to blood pressure [30]. To distinguish from the vascular elastin, we refer to cardiac elastin as the elastin in the heart separate from vascular elastin in the coronary vasculature system. Literature review showed that cardiac elastin has not been well investigated, and there is still a substantial knowledge gap in its detailed anatomical characteristics, microstructure, and biomechanical roles.

Nevertheless, recent reports have shed light on the possible biomechanical roles of cardiac elastin on heart functions [22,31–33]. It was noted that the overexpression of elastin in an infarcted heart could efficiently help prevent scar expansion, stabilize tissue structure, and delay ventricular dysfunction [31,32]. Moreover, the change in collagen-to-elastin ratio, and not collagen alone, was believed to be correlated with the stiffening of cardiac tissues due to either aging or certain pathological conditions [22,33]. Some research also showed that the loss of contractile function in either native or diseased myocardium might partially result from the reduction in elastin contents of the cardiac tissues [22,31,34–38]. Most recently, our study on healthy native porcine hearts has revealed a novel phenomenon - the epicardial layer, rich in elastin, acts like a prestrained “balloon” that wraps around the heart left ventricle (LV) [39]. Via a finite element model, we further demonstrated that it is the prestraining of the epicardial layer, not the epicardial layer alone, providing (1) additional resistance against LV diastolic expansion and (2) ventricular wall protection by reducing myocardial stress [39]. From a biomechanical perspective, the epicardial prestrained confinement can provide an additional resistance mechanism during LV diastolic expansion and assist the contraction of the LV by epicardial recoiling.

The above-mentioned roles of elastin in cardiac biomechanics warrants an in-depth understanding of the existence and status of cardiac elastin in hearts, as well as how the structural characteristics of cardiac

elastin are related with the mechanical properties of ventricular wall. For cardiac elastin, a previous histological study in rat reported that elastin fibers are prevalent around the epicardial layer and endocardial layer of both ventricles and atria, and were believed to have no apparent difference in the histological staining patterns of the four chambers [40]. A recent two-photon microscopic study on the porcine hearts reported that the elastin fibers in the epicardium were aligned in parallel with local collagen fibers and the elastin fibers in the endocardium took a diffuse pattern [26]. In the myocardium, the elastin fibers were reported as sparsely observed in the non-vascular regions [22,40].

These reports suggest the structure of cardiac elastin, such as spatial distribution, microstructure, and network morphology in the ventricular wall, needs to be further investigated and described. In this study, we aim address this knowledge gap by thoroughly characterizing the cardiac elastin network of the porcine left ventricle, including epicardial elastin, interstitial elastin (elastin in myocardium), endocardial elastin, and elastin associated with Purkinje cells. We chose porcine heart model because it is the closest and validated model to human heart in anatomy, physiology, and function [41–43]. For epicardial elastin, laser scanning confocal microscopy (LSCM) was applied to obtain 3D image stacks of the elastin fiber network, which was able to generate high quality signals due to more distinguishable fibrous features. For the sparsely-distributed myocardial elastin fibers, dense endocardial elastin fibers, and fine elastin associated with Purkinje cells, Movat’s pentachrome histology was performed to reveal the detailed distribution and morphology of those elastin fibers. The obtained knowledge provides an essential structural basis for better understanding the biomechanical roles of elastin in various anatomic components of the hearts. The detailed spatial distribution and network morphology of cardiac elastin in healthy hearts also sets an elastin-related benchmark for understanding heart physiology and pathophysiology, and serves as a biomimicking target of in cardiac tissue engineering and bioactive material design.

## 2. Materials and methods

### 2.1. Epicardial elastin mapping and characterization

**Epicardial tissue preparation.** Fresh porcine hearts (Yorkshire, ~ 6-month-old) were obtained from a local slaughterhouse and transported in 1X PBS at 4 °C to the laboratory. Four porcine hearts were used for laser scanning confocal microscopy (LSCM) imaging of the epicardial elastin. Square samples (~10 mm × 10 mm × 1 mm) that cover the base, middle, and apex regions were dissected from the left ventricle of each fresh native heart (Fig. 1-A,B). For the base region, five locations were examined, with two covering the anterior area, one covering the lateral area, and two covering the posterior area. For the middle region, four locations were examined, with two covering the anterior area, one covering the lateral area, and one covering the posterior area. For the apex region, three locations were examined, with one covering the area adjacent to anterior, one covering the true apex, and one covering the area adjacent to the posterior wall (Fig. 1-A,B). Note that one edge of the square sample was aligned along the circumferential direction of the ventricle, and the other edge aligned along the longitudinal direction. All samples were marked with a suture at the upper right corner to distinguish sample orientation. Moreover, accurate dimensions of the square samples were recorded before further process using a Mitutoyo digital caliper.

**Decellularization.** To improve the penetration depth of laser light, an optimized version of our established decellularization method [44] was used to remove the cells in the epicardial layer while preserving the cardiac ECM microstructure. Fresh native samples were subjected to decellularization in a rotating bioreactor using 1% sodium dodecyl sulfate (SDS) with 0.01% trypsin, 1 mM phenylmethylsulfonyl fluoride (protease inhibitor), 1% antibiotics (100 U/ml penicillin and 100 µg/ml streptomycin), 20 µg/ml RNase A and 0.2 mg/ml DNase at room

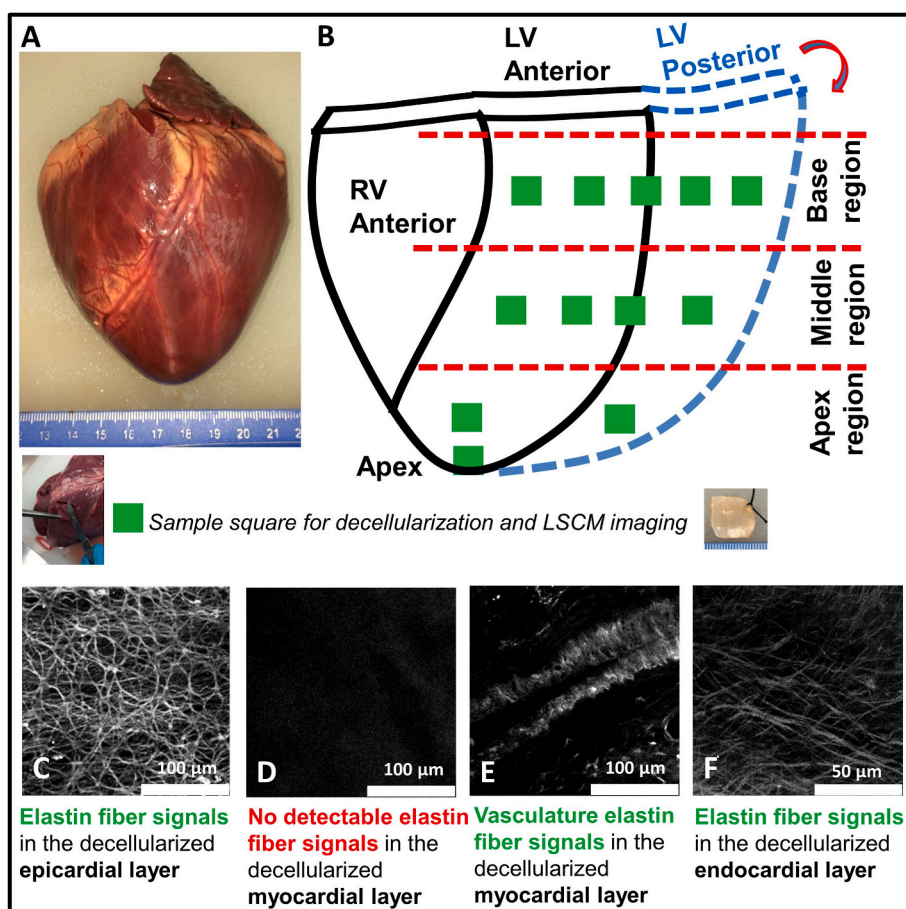


**Fig. 1.** Schematic illustration of the heart left ventricle shows the locations of sample dissection (A, B) and verifications of elastin signal specificity (C–F). Dashed lines (B) label three regions (base, middle and apex) of the left ventricle with five locations examined in the base region (two covering the anterior area, one covering the lateral area, and two covering the posterior area), four locations examined in the middle region (two covering the anterior area, one covering the lateral area, and one covering the posterior area), three locations examined in the apex region (one covering the area adjacent to anterior, one covering the apex tip, and one covering the area adjacent to posterior). Elastin fiber signals were generated by autofluorescence of elastin under CY3 channel (Ex = 543 nm). Abundant elastin signals were detected in the epicardial layer (C), the endocardial layer (F), and the region associated with blood vessels (E). There was no detectable elastin signal in the acellular, collagen-dominated myocardial layer (D).

temperature for 1 week. The decellularization solution was changed every two days to avoid contamination and tissue deterioration. After samples were fully decellularized, sample dimensions (length, width, and thickness) were measured to verify the degree of dimension preservation. After the PBS wash, the decellularized samples were subjected to a gradient glycerol treatment protocol, in which samples were treated for 30 min at each step in PBS solutions with 25% glycerol, 50% glycerol, 75% glycerol, and lastly 100% (pure) glycerol to obtain clear and transparent samples. The transparency of tissue sample was able to enhance the laser light penetration depth, and the effectiveness of this protocol was also verified by previous laser confocal and laser scattering studies on soft tissues [45].

**Laser scanning confocal microscopy (LSCM).** The glycerol-treated acellular samples were subjected to LSCM (Zeiss Inc., Inverted mode, Axiovert 200 M) to image the 3D elastin network under CY3 channel (elastin autofluorescence, Ex = 543 nm) using a z-stack imaging technique. Due to the scarce existence, finer fiber, and low density of interstitial elastin in myocardium, LSCM showed limited capacity to detect the elastin specific signal from the decellularized myocardial layer (Fig. 1-D). Moreover, we noticed that the elastin specific LSCM signal from the endocardium layer was diffuse and blurred (elastin specific signal overlapping) due to the finer and much denser endocardial elastin network. We hence focused 3D mapping only on the epicardial elastin fibers at the current stage. Starting from the epicardial surface, the 3D z-stack images covered a total thickness of  $\sim 70 \mu\text{m}$  at  $\sim 1 \mu\text{m}$  interval. All images were acquired with a 12-bit gray scale and a dimension of  $1024 \times 1024$  pixels. ImageJ (NIH, Bethesda, MD) was used to create 3D projections of the first 15  $\mu\text{m}$  section, the last 15  $\mu\text{m}$  section, and the full thickness of each image stack. Elastin fiber orientation and distribution in different layers were quantified using the OrientationJ plugin.

## 2.2. Histological assessments for epicardial elastin, myocardial elastin, endocardial elastin, and elastin associated with Purkinje fibers

Five porcine hearts (Yorkshire,  $\sim 6$ -month-old) were used for histological study. Epicardial, myocardial, and endocardial samples were dissected from the left ventricle anterior wall of the native porcine hearts. Note that there was no decellularization performed for histological study. For endocardial samples, since the size and morphology of the trabeculae carneae (ridges) varied greatly, we chose the regions between the trabeculae ridges that were relatively smooth in order to get a more consistent representation of the endocardial surface. The dissected samples were fixed in 10% buffered formaldehyde solution for 72 h to fully preserve the tissue morphology [46,47], dehydrated with graduated concentrations of ethanol, and embedded in paraffin. Cross-sectional slices of 5  $\mu\text{m}$  thickness were then obtained from the fixed tissue samples via a microtome machine and stained with Movat's pentachrome protocol, in which elastin was stained black, collagen stained yellow, heart muscle stained red, and Purkinje fibers stained pale pink. The histological slices were then imaged using a bright field microscope (Nikon EC600).

## 3. Results

### 3.1. Epicardial sample dimensions before and after decellularization

The sample dimensions (length, width, and thickness) of the dissected epicardial layer were measured before and after decellularization, and the percent reductions after decellularization are listed in Table 1. Average reductions of 10.47% in the circumferential direction, 17.86% in the longitudinal direction, and 20.09% in thickness were observed (Table 1). Our data showed that the dimension reductions

**Table 1**

Sample dimensions measured before and after decellularization and the percent reductions after decellularization. CD, LD, and T represent the length of circumferential direction, length of longitudinal direction, and thickness of each sample, respectively.

Unit: mm	Native Samples			Decellularized Samples			Percentage reduction, %		
	CD	LD	T	CD	LD	T	CD	LD	T
1	20.12	15.54	1.02	17.98	13.33	0.80	11.18%	14.22%	21.41%
2	18.54	14.75	0.88	16.09	11.79	0.70	13.21%	20.07%	20.06%
3	19.63	12.26	0.93	18.40	9.08	0.77	6.26%	25.94%	17.20%
4	15.87	10.27	0.99	14.10	8.31	0.81	11.15%	19.08%	18.18%
5	13.58	7.99	0.86	11.47	6.23	0.68	15.54%	22.03%	20.47%
6	18.00	10.67	0.97	16.63	9.15	0.71	7.61%	14.25%	26.42%
7	14.50	9.49	0.93	12.40	7.82	0.72	14.48%	17.60%	22.16%
8	16.95	14.23	0.96	15.57	11.47	0.84	8.14%	19.40%	12.50%
9	14.92	12.07	1.01	13.93	11.08	0.78	6.64%	8.20%	22.39%
				Average			10.47%	17.86%	20.09%

were reasonably small and mainly from the removal of the attached myocardium during decellularization, indicating the epicardial layer was preserved relatively well.

**3.2. Elastin specificity of the obtained LSCM signal**

Elastin autofluorescence has been widely used in confocal imaging [48,49]. To validate that the signals are elastin specific, we compared the LSCM images of the decellularized epicardial layer, myocardium, myocardial region with blood vessels, and the endocardial layer. We demonstrated that the fiber network signals in the epicardial layer (Fig. 1C) and the endocardial layer (Fig. 1F) were abundant and showed a morphology consistent with our histological observation (Figs. 6 and 7). However, in the decellularized myocardial layer where collagen network is dominant and elastin fibers are sparse and thin, no strong elastin signal was detected (Fig. 1D). In the myocardial region with blood vessel, the elastin signals from the vascular were readily observed, delineating the contour and morphology of the blood vessel (Fig. 1E).

**3.3. Mapping of the epicardial elastin with LSCM**

For all the imaging locations, we created three projections (the superficial first 15 μm thickness, the deepest last 15 μm thickness, and full epicardial thickness) from the image stacks and quantified their corresponding elastin fiber orientation and distribution (Figs. 3–5). The full thickness projection could reveal an overall trend of the elastin fiber network, and the first 15 μm thickness projection and last 15 μm thickens projection could provide depth-dependent information of the elastin fibers. For the fiber distribution curve, the circumferential

direction of ventricle, i.e., horizontal direction of the image, was defined as 0° angle.

With the full thickness projections, the LV epicardial elastin networks were mapped in Fig. 2 using representative images, and the orientation measurements were presented as Mean ± Standard Deviation in Table 2. We noticed that the epicardial elastin fiber networks had an overall fiber orientation that were associated with the helical myocardial fiber orientation spanning from the base to the apex (Fig. 2).

**Table 2**

Epicardial elastin fiber orientation presented as Mean ± Standard Deviation. The orientation data were obtained from the full thickness projection of each location, covering LV base region, LV middle region, and LV apex region. The circumferential direction of ventricle, i.e., horizontal direction of the image, was defined as 0° angle. Four porcine hearts were used for the orientation measurement.

N = 4		Epicardial Elastin Fiber Orientation (Mean ± Standard Deviation)
Unit: degree (°)		
Base region	B1	-8.9 ± 8.4
	B2	-48.8 ± 5.9
	B3	14.5 ± 18.4
	B4	-1.5 ± 2.8
	B5	-6.0 ± 0.7
Middle region	M1	-26.8 ± 35.4
	M2	-64.2 ± 22.0
	M3	-1.0 ± 0.7
	M4	-33.5 ± 1.4
Apex region	A1	-70.5 ± 1.4
	A2	-1.8 ± 4.7
	A3	-82.8 ± 3.9

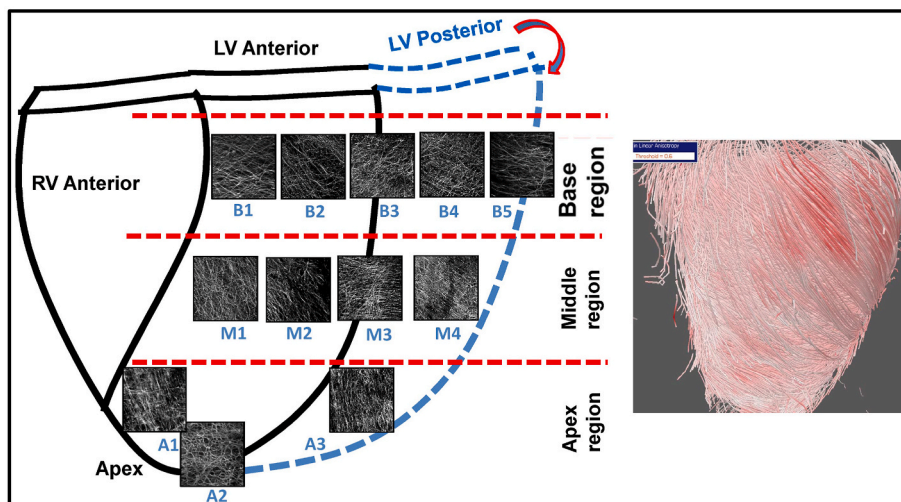


**Fig. 2.** The overall distribution of epicardial elastin network in three regions (base, middle, and apex) of the left ventricle was obtained using the 3D laser scanning confocal microscopy (LSCM). The top region (B1–B5) and middle region (M1–M4) show the epicardium samples that cover each region from the anterior side to the posterior side. The bottom region (A1–A3) represents the epicardium samples around/on the apex region. Right panel shows the multilayered helical structure of the heart muscle fibers revealed by our previous Diffusion-Tensor Magnetic Resonance Imaging (DT-MRI) study [59]. We noticed that the overall architecture of the epicardial elastin network from the base to the apex has certain correlation with the helical structure of the heart muscle fibers.

The elastin fibers in the base region showed a degree of multidirectional reinforcement, with an overall wrapping trend along the circumferential direction (Fig. 3A,D,E). The B1 region (basal anterior) had an overall orientation at  $-8.9 \pm 8.4^\circ$  (Fig. 3A, Table 2). The B2 region (basal anterior) showed an oblique orientation of  $-48.8 \pm 5.9^\circ$ , downwards-pointing and aligning with the heart muscle helical orientation (Fig. 3B, Table 2). On the basal lateral side (B3), elastin fibers showed a more random pattern with a slightly  $14.5 \pm 18.4^\circ$  upwards-pointing trend (Fig. 3C, Table 2). The overall orientations for B4 and B5 (basal posteriors) were  $-1.5 \pm 2.8^\circ$  and  $-6.0 \pm 0.7^\circ$ , respectively (Fig. 3D and E, Table 2).

All the basal locations (B1–B5) clearly demonstrated depth variation of the elastin network structure, as shown by different overall fiber orientation, the degree of alignment, and fiber interconnections when compared the first 15  $\mu\text{m}$  thickness to the last 15  $\mu\text{m}$  thickness (Fig. 3A–E). We found that in the basal anterior B1 (Fig. 3A), the first 15  $\mu\text{m}$  layer showed an overall circumferential orientation slightly pointing downwards and was more random when compared to the last 15  $\mu\text{m}$  layer, which was slightly pointing upwards and more aligned. In the basal anterior B2 (Fig. 3B), elastin fibers in the first 15  $\mu\text{m}$  layer were highly aligned and pointing downwards, while more random aligned in the last 15  $\mu\text{m}$ . Elastin fibers in the basal lateral B3 (Fig. 3C) showed a slight upwards orientation in the first 15  $\mu\text{m}$  thickness and a more random alignment in the last 15  $\mu\text{m}$  thickness. In the basal posterior B4 (Fig. 3D), the random distribution of elastin fibers was observed in both the first 15  $\mu\text{m}$  thickness and the last 15  $\mu\text{m}$  thickness. In the basal posterior B5 (Fig. 3E), a strong circumferential alignment slightly pointing downwards was found in the first 15  $\mu\text{m}$  layer, while a random orientation in the last 15  $\mu\text{m}$  layer.

In the middle region, elastin fibers in M1 and M2 regions (middle anterior) displayed a more obvious oblique orientation pointing downwards with a  $-26.8 \pm 35.4^\circ$  and  $-64.2 \pm 22.0^\circ$  angle, respectively (Fig. 4A and B, Table 2). For both M1 and M2, the deeper layer was more aligned than the surface layer (Fig. 4A and B). At the M3 region (middle lateral), the overall orientation was  $-1.0 \pm 0.7^\circ$ , with the deeper layer showing an upwards pointing angle and the surface layer showing a more circumferentially wrapping fiber orientation (Fig. 4C). For the M4

region (middle posterior), the elastin fibers exhibited an overall  $-33.5 \pm 1.4^\circ$  downwards-pointing orientation, and the last 15  $\mu\text{m}$  layer elastin fibers exhibited a more random orientation than the first 15  $\mu\text{m}$  layer (Fig. 4D).

When approaching the apex, A1 region (adjacent to apex in anterior side, Fig. 5A) and A3 region (adjacent to apex in posterior side, Fig. 5C) showed a  $-70.5 \pm 1.4^\circ$  and  $-82.8 \pm 3.9^\circ$  downwards orientation (almost longitudinal) convergent to the tip of the apex, respectively (Table 2). In the tip of the apex region (Fig. 5B), the deeper layer had a  $-1.8 \pm 4.7^\circ$  orientation (Table 2) that seemed to bridge the anterior wall fibers to the posterior wall fibers in a 3D manner. In contrast, the elastin fibers on the surface of the apex tip exhibited a randomly-meshed network feature, with wavy elastin fibers interconnected to form pore-like structure (Fig. 5B).

### 3.4. Histological characteristics of cardiac elastin

**Elastin network in the epicardial layer.** Histological images of Movat's pentachrome staining revealed significant differences in network morphology and microstructure between the epicardial elastin network and the endocardial elastin network (Figs. 6 and 7). In the epicardial layer (Fig. 6A–D), elastin fibers (black color) were associated with collagen (yellow color), and the thickness of epicardial layer varied from  $\sim 50 \mu\text{m}$  to  $\sim 200 \mu\text{m}$  (Fig. 6A–D). The staining of epicardial elastin fibers showed a thick and distinguishable fibrous structure, with a wavy and meshed configuration (Fig. 6A–D). Moreover, in those epicardial histological images, the long elastin threads showed the fibers with in-plane orientation and the short elastin threads showed the fibers with out-of-plane orientation, confirming the multidirectional orientation and depth-dependency observed by LSCM (Fig. 4).

**Elastin network in the endocardial layer.** The elastin network patterns in the endocardial layer demonstrated clear differences when compared to the elastin network in the epicardial layer (Fig. 7A–D). First, the endocardial layer had areas where it was more undulating (Fig. 7A and B) and locations where it was relatively smooth (Fig. 7C and D). The thickness of the endocardial layer varied from  $\sim 100 \mu\text{m}$  to  $\sim 250 \mu\text{m}$ , and Movat's pentachrome staining revealed a higher elastin-

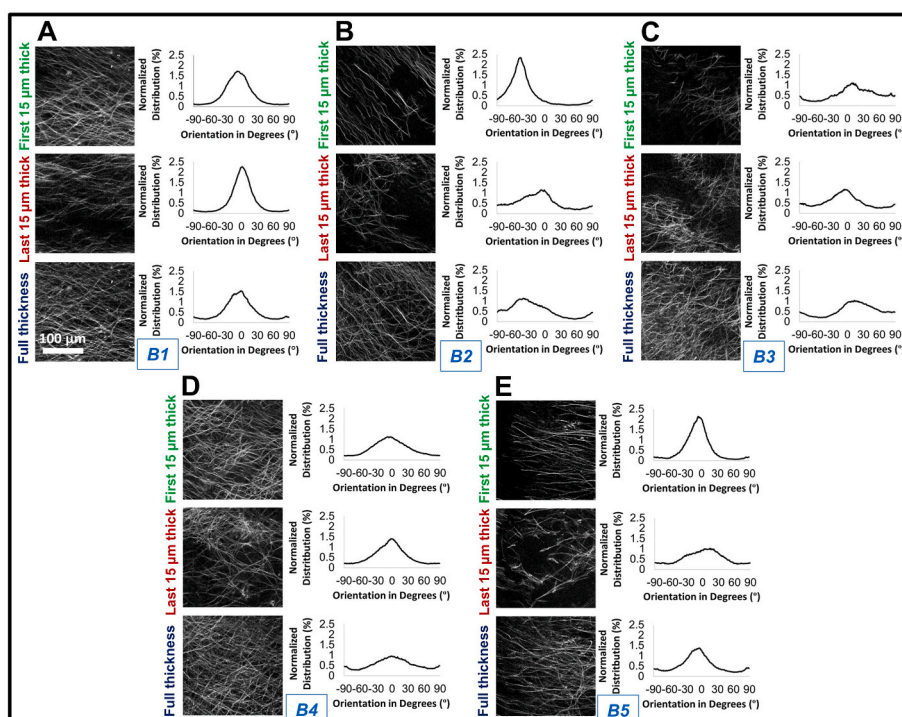


**Fig. 3.** Layered epicardial elastin network in the base region of the left ventricle. Projections and normalized fiber distributions were obtained from the locations of basal anterior B1 (A) and B2 (B), basal lateral B3 (C), and basal posterior B4 (D) and B5 (E). Top panel: projections of the first 15  $\mu\text{m}$  thick layer (the surface into the 15  $\mu\text{m}$  deep of the sample); middle panel: projections the last 15  $\mu\text{m}$  thick layer (the last 15  $\mu\text{m}$  into the opposite side of the surface); bottom panel: projections of the full thickness of the sample. Scale bar = 100  $\mu\text{m}$ .

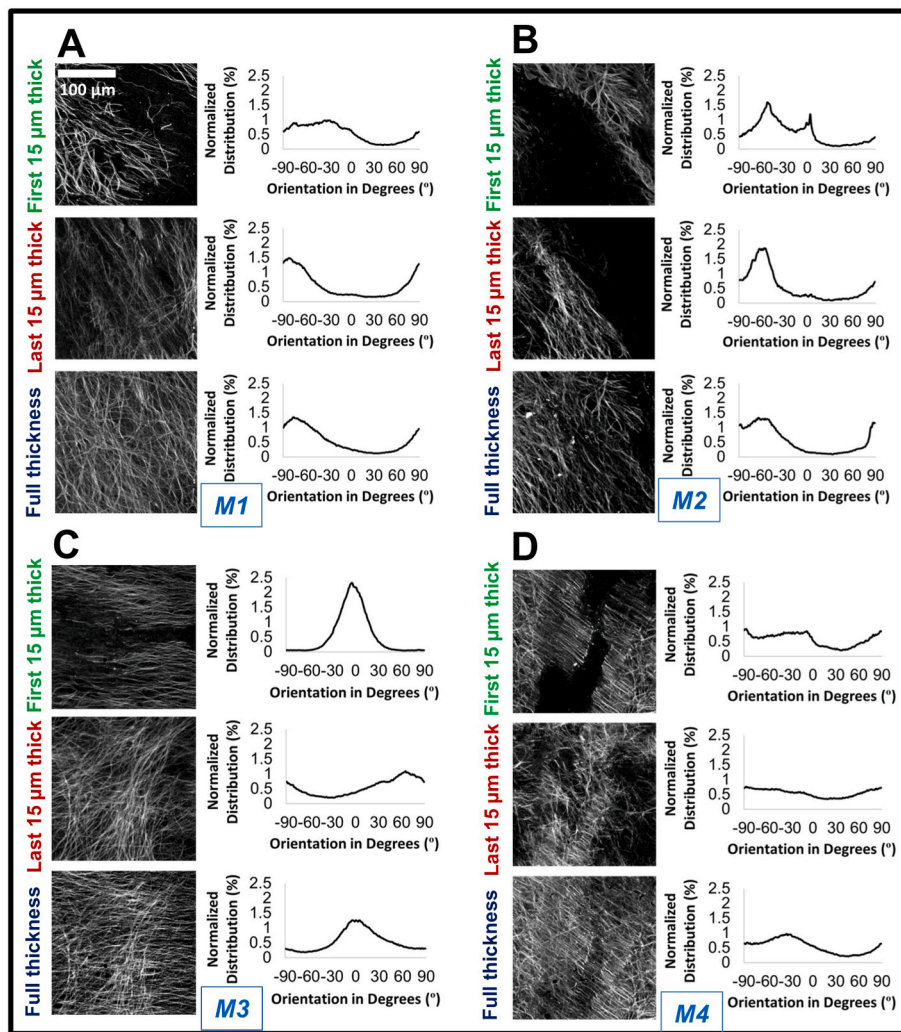


Fig. 4. Layered epicardial elastin network in the middle region of the left ventricle. Projections and normalized fiber distributions were obtained from the locations of middle anterior M1 (A) and M2 (B), middle lateral M3 (C), and middle posterior M4 (D). Top panel: projections of the first 15 μm thick layer (the surface into the 15 μm deep of the sample); middle panel: projections the last 15 μm thick layer (the last 15 μm into the opposite side of the surface); bottom panel: projections of the full thickness of the sample. Scale bar = 100 μm.

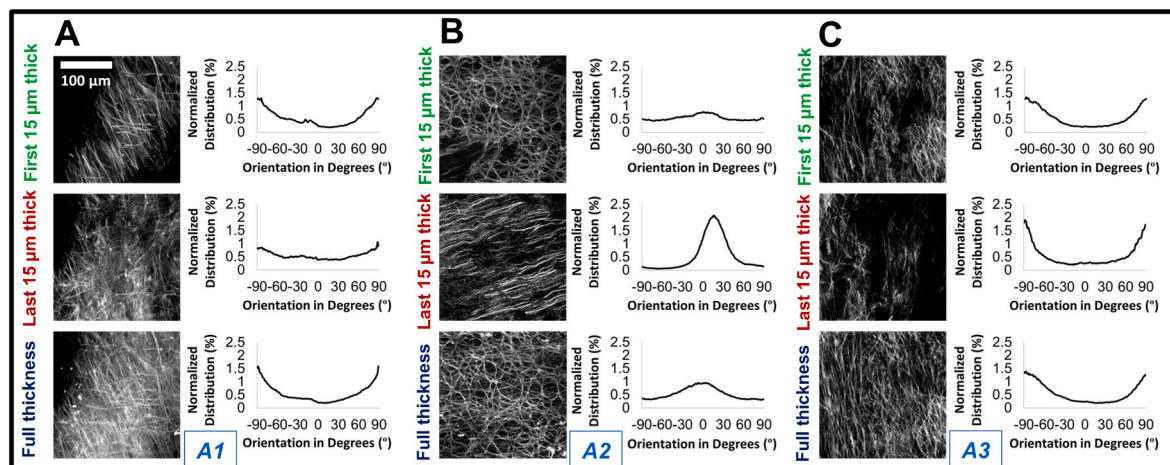
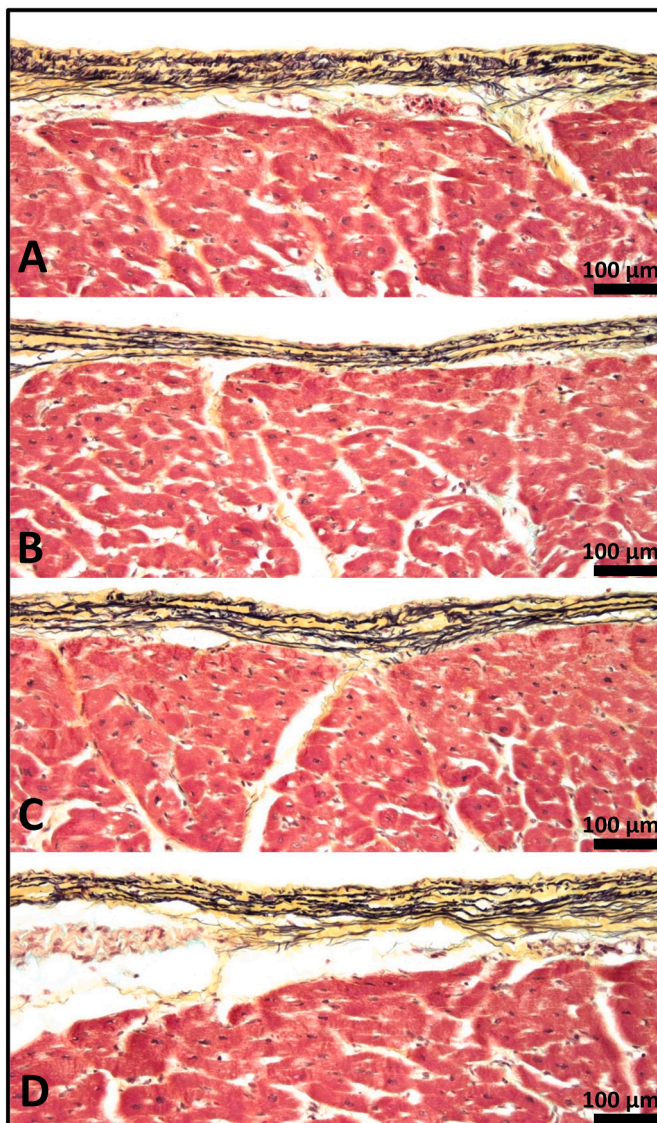


Fig. 5. Layered epicardial elastin network in the apex region of the left ventricle. Projections and normalized fiber distributions were obtained from the locations of apex anterior A1 (A), apex point A2 (B), and apex posterior A3 (C). Top panel: projections of the first 15 μm thick layer (the surface into the 15 μm deep of the sample); middle panel: projections the last 15 μm thick layer (the last 15 μm into the opposite side of the surface); bottom panel: projections of the full thickness of the sample. Scale bar = 100 μm.

collagen ratio (black: elastin, yellow: collagen) (Fig. 7A–D). Second, the elastin fibers in the endocardial layer were finer and formed much denser networks, with a higher degree of waviness when compared to

the epicardial elastin network (Fig. 7). Lastly, the in-plane oriented elastin fiber bundles (long threads) and the out-of-plane orientated elastin fiber bundles (short, aligned threads) revealed that the



**Fig. 6.** Histological images of the LV cross-sections of the native porcine hearts showed the microstructure of the epicardial layer (A–D). Epicardial elastin fibers covered a thickness range of 50  $\mu\text{m}$ –200  $\mu\text{m}$  and showed location-dependency and depth-dependency. The epicardial elastin fibers exhibited thick and distinguishable fibrous structure, with a wavy and meshed configuration. Movat’s pentachrome staining: Collagen in yellow, elastin fibers in black, and cardiac muscles in red. Scale bar = 100  $\mu\text{m}$ .

endocardial elastin also had a depth-dependency in fiber alignment and orientation (Fig. 7A–D). Note that Purkinje fibers (pale pink staining) were identified between the endocardium and the myocardium (red staining) (Fig. 7A–D). We noticed that the Purkinje cells were closely surrounded by collagen and fine elastin fibers (Fig. 7, arrows). Note that more details about Purkinje cell-associated elastin were provided in Fig. 10.

**Interstitial elastin in the myocardium.** Movat’s pentachrome staining was able to detect the myocardial interstitial elastin fibers, which were finer and less frequently existing (Fig. 8). A closer examination of the histological images showed that the fine interstitial elastin fibers in the myocardium were associated with the perimysial collagen that wraps around heart muscle bundles (Fig. 8A–D). Groups of parallel-aligned elastin fibers (black color) were observed in-between muscle bundles and embedded in the perimysial collagen (yellow color), with a locally aligned, “hinge”-like morphology (Fig. 8C–F, rectangles). Vascular elastin was observed in the walls of the blood vessels,

especially in the intima layer (Fig. 9A,C, arrows). In the collagen network that meshes the blood vessels to the surrounding myocardium, abundant interstitial elastin fibers existed, and this part of interstitial elastin fibers were more associate with the anatomical anchoring of the cardiac vasculature (Fig. 9B,D, rectangles). Note that the histological imaging was not able to detect the ultrafine elastin in the endomysial collagen (Type I and Type III) that ensheathes each individual muscle fiber [50,51].

**Elastin fibers associated with Purkinje fibers.** Located in the sub-endocardium and branching into myocardium, Purkinje fibers and their branches are responsible for the electrical conduction by sending electrical impulses to cardiomyocytes in the ventricles of the heart [52]. Most of the anatomical studies on Purkinje fibers focused on fiber spatial distributions and morphologies of Purkinje cells, which are larger in size than cardiomyocytes, have more mitochondria but fewer myofibrils when compared to cardiomyocytes, and are interconnected by desmosomes and gap junctions without intercalated discs [53,54]. By imaging the slow tonic myosin heavy chain in Purkinje fibers with immunofluorescence staining, Pennisi et al. compared the cellular morphologies of (i) the subendocardial Purkinje fibers, (ii) the branch point extended from the subendocardial Purkinje fibers, and (iii) the intramural Purkinje fibers (situated in and surrounded by myocardium) [55].

Fig. 10 captured some interesting microstructural details on how ECM was associated with Purkinje fibers. We found that the fine elastin fibers, meshing with collagen, morphologically wrapped around groups of Purkinje cells (cell groups in cross-sectional view) (Fig. 10A, red arrow). Furthermore, the fine elastin fiber arrays, which had local alignment, were also frequently observed existing between the Purkinje cells, and these elastin fiber arrays always seemed to associate with yellow-stained collagen (Fig. 10B,C, blue arrows). Morphologically, those interstitial elastin and collagen seemed to bind the Purkinje cells together, likely enabling the cell assembly a fibrous feature. As shown in Figs. 7 and 10, we captured the elastin fibers and collagen (i) that were associated with the subendocardial Purkinje fibers (Figs. 7 and 10A), (ii) that were associated with the branch point extended from subendocardial Purkinje fibers (Fig. 10B, green arrow, T-shape branching), and (iii) that were associated with the intramural Purkinje fibers (Fig. 10C, yellow arrow)

## 4. Discussion

### 4.1. Mapping of the epicardial elastin fiber network

We have successfully imaged and mapped the elastin fiber network in the LV epicardial layer using LSCM, which has been widely used for imaging elastin fiber distribution in various tissues, such as blood vessels, heart valves, and lungs [56–58]. With a penetration depth of  $\sim 70$   $\mu\text{m}$  achieved by our approach, we were able to demonstrate that the epicardial elastin fiber networks in the LV were highly location and depth-dependent. For the depth-dependency, we revealed that elastin fibers often changed their overall orientation and degree of alignment throughout the epicardial thickness (Fig. 3); moreover, this layered variation was further confirmed by histological observation on cross-sectional slices (Fig. 6). For the location-dependency, we noticed that the overall architecture of the epicardial elastin network from the base to the apex (Fig. 2 left panel) has certain correlation with the multilayered helical structure of the heart muscle fibers, which was revealed by our previous Diffusion-Tensor Magnetic Resonance Imaging (DT-MRI) study (Fig. 2 right panel) [59].

For the LV anterior wall, we found that elastin fibers had an overall circumferential wrapping orientation in the base region, took a more apex-inclined orientation in the middle region, and had the most vertical fiber alignment when nearing the apex. Similarly, on the posterior LV elastin fibers had an overall horizontal alignment in the base region, to a more apex-inclined orientation in the middle region, and then a highly vertical alignment when nearing the apex. The location variation of

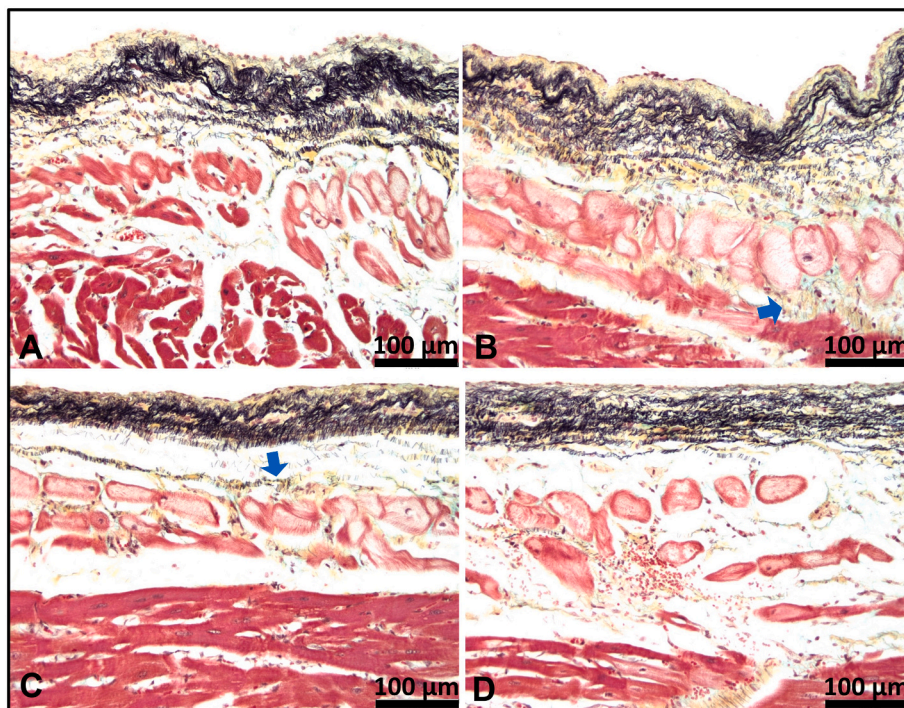


**Fig. 7.** Histological images of the LV cross-sections of the native porcine hearts showed the ultrastructure of the endocardial layer (A–D). Endocardial elastin fibers covered a thickness range of 100  $\mu\text{m}$ –250  $\mu\text{m}$  and showed location-dependency and depth-dependency. The endocardial elastin fibers were finer and formed much denser networks, with a higher degree of waviness when compared to the epicardial elastin network. Note that Purkinje fibers (pale pink staining) were identified beneath the endocardial layer and above the myocardium (red staining). We noticed that the Purkinje cells were also associated with fine collagen and elastin fibers (Arrows). Movat's pentachrome staining: Collagen in yellow, elastin fibers in black, cardiac muscles in red, and the Purkinje fibers in pale pink. Scale bar = 100  $\mu\text{m}$ .

epicardial elastin fiber network could very likely be part of the structural mechanisms that contributed to the location-dependency of the epicardial prestrain and residual stress as reported in our recent paper [39].

#### 4.2. Elastin fiber network in the endocardial layer and interstitial elastin fibers in the myocardium

**Endocardial elastin fiber network.** Due to the challenges in LSCM, i. e., diffusive elastin signal in endocardium and lack of the elastin signal in myocardium, we had to use histological analysis to investigate the morphologies of elastin fiber network in the endocardial layer and the interstitial elastin fibers in the myocardium. As shown by histology, the elastin fibers in the endocardial layer were finer and much denser (Fig. 7A–E) than the epicardial elastin fibers (Fig. 6A–E), thus resulting in LSCM signals from the endocardial elastin fibers being overlapped in a diffusive manner. This signal overlapping makes it difficult to distinguish individual endocardial elastin fibers, and perform 3D imaging and analysis at this stage.

When compared to the epicardial layer, the endocardial layer was thicker ( $\sim 100\ \mu\text{m}$ – $\sim 250\ \mu\text{m}$ ) and had a higher elastin-collagen ratio and denser elastin fiber network; moreover, endocardial elastin fibers were finer and more wavy than the epicardial elastin fibers (Fig. 7A–D). Those drastic microstructural differences might be related with the different interface mechanics associated with the endocardial surface and epicardial surface, such as the ranges of deformation experienced by those surfaces during ventricular expansion and contraction. More in-depth studies are needed to reveal the underlying structural-functional reasons of why elastin network in those two interface layers adapt its unique morphology.

Note that the endocardial samples used for histological assessment had a relatively smooth surface. Even in those smooth regions, the epicardial layer showed various microscopic morphologies, including highly undulating elastin layer (Fig. 7A and B) and relatively smooth elastin layer (Fig. 7C and D), signifying other microscopic morphologies might exist in the trabeculae columns. Future study will hence examine the endocardial layer of the irregular, projected trabeculae columns, to reveal the elastin fiber features associated with these projected columns.

**Interstitial elastin fibers in the myocardium.** For the myocardium,

the LSCM signals from the elastin fibers were very weak and difficult to detect due to the sparse distribution of the interstitial elastin fibers. As shown by our histological images, myocardial interstitial elastin were fine fibers associated with the perimysial collagen and were widely-separated by the heart muscle bundles (Fig. 8). The co-existence of the interstitial elastin fibers with the perimysial collagen indicated the functional roles of perimysial elastin fibers in binding and connecting heart muscle bundles. Moreover, the locally-aligned, hinge-like elastin fiber array between heart muscle bundles suggest possible mechanical roles of interstitial elastin fibers in (i) participating force transfer in myocardial passive loading during diastolic phase, and (ii) assisting recoil during systolic phase by releasing the elastic energy stored during stretching.

One can speculate that optimal inter-muscle bundle connection should have both collagen network and interwoven elastin fibers, with the collagen fibers providing mechanical strength and elastin fibers facilitating recoiling that is important in dynamic loading and unloading cycles. Without elastin fibers, the pure collagen network would possibly have an inferior performance in mediating the dynamic inter-muscle bundle connection. Indeed, this mechanical role of interstitial elastin in mediating ventricular wall functional behavior is consistent with a prior observation in MI scar tissues that investigated its elastin expression/content. In this study, the overexpression of elastin in an infarcted heart efficiently prevented scar expansion, stabilized tissue structure, and delayed ventricular dysfunction [31,32,60]. There was also research showing that the loss of contractile function in the native or diseased myocardium might partially result from the reduction in elastin content of the cardiac tissues [22,31,34–38].

Via histological imaging method, the ultrafine elastin fibers were not detectable in the endomysial collagen (Type I and Type III) that ensheathes each individual muscle fiber (Fig. 8A–D). Higher resolution imaging technique such as Transmission Electron Microscopy (TEM) and immunohistochemical staining will be needed to assess how the ultrafine elastin fibers were associated with the endomysial collagen (Type I and Type III). According to TEM observation from Robinson et al., ultrafine elastic fibers, along with collagen fibers, interconnect heart muscle fibers and helically wind around myocytes [50,51]. It is worthy to point out that the elastin content in the myocardial layer indeed is not

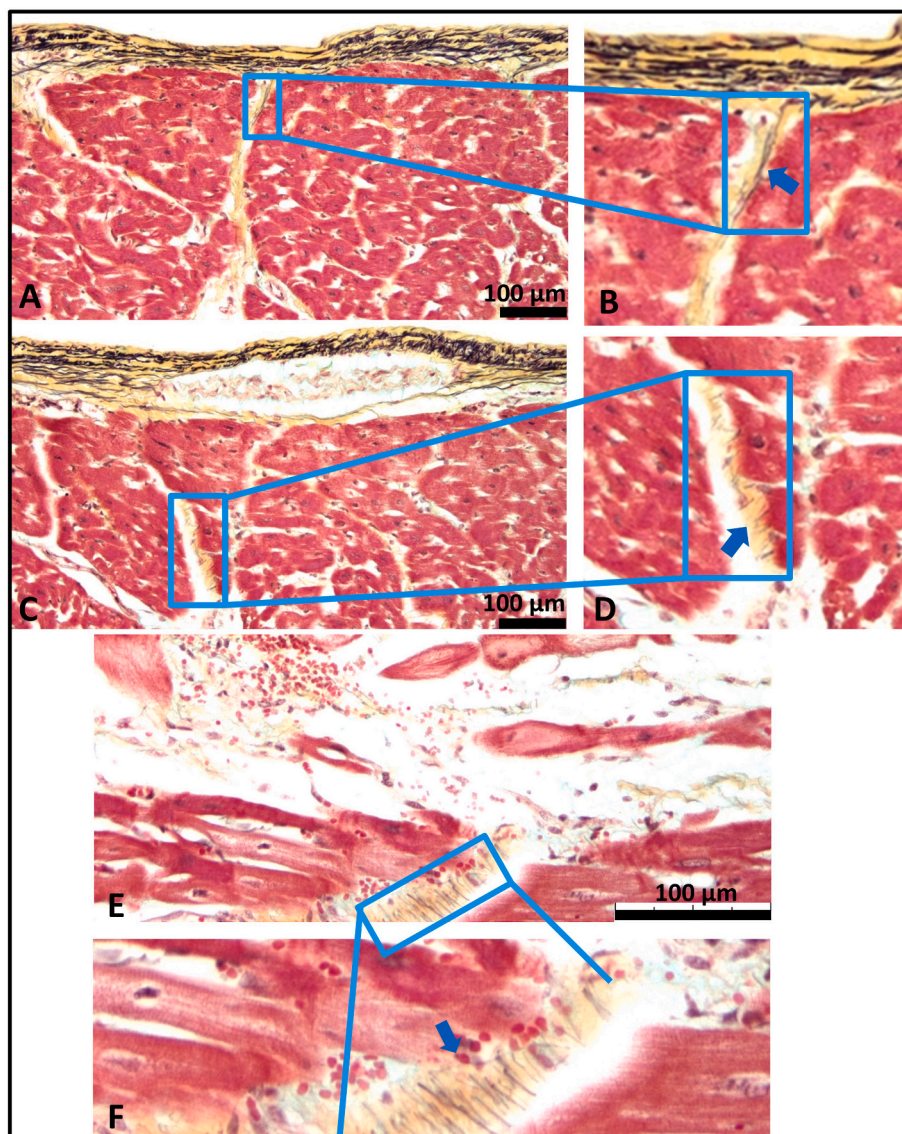


**Fig. 8.** Histological images of the LV myocardium cross-sections of the native porcine hearts, with myocardial interstitial elastin fiber morphology revealed. The interstitial elastin fibers in the myocardium were found to co-exist with the perimysial collagen to bind the cardiomyocyte bundles, and some of the interstitial elastin fibers even showed locally aligned, hinge-like structures to connect the adjacent cardiomyocyte bundles. Arrows in **B** and **D** labeled the detailed interstitial elastin fiber structure (**B** and **D** were the zoomed-in images of the rectangular boxes in **A** and **C**). Arrows in **F** points out locally aligned, hinge-like elastin fiber structure that connected the adjacent cardiomyocyte bundles (**F** was the zoomed-in image of the rectangular box in **E**). Movat's pentachrome staining: Collagen in yellow, elastin fibers in black, and cardiac muscles in red. Scale bar = 100  $\mu\text{m}$ .

trivial due to its existence in the following sources. The elastin sources in the myocardial layer include (i) fine interstitial elastin fibers that interconnect the heart muscle bundles (Fig. 8), (ii) ultrafine interstitial elastin fibers that surround the individual muscle fiber [50,51], (iii) elastin fibers in coronary arteries/arterioles that are plenty in myocardium (Fig. 9), and (iv) interstitial elastin fibers that help anchoring coronary blood vessels to the surrounding tissues (Fig. 9)."

#### 4.3. Elastin fibers associated with Purkinje cells

Histological images revealed that cardiac elastin fibers, along with collagen fibers, closely interweaved with the Purkinje cells. Deducing from the morphology, these interstitial elastin and collagen could participate in organizing cardiac Purkinje cells into "fibrous" and "branching" features, as well as serve as a protective mechanism when the electrically conductive Purkinje fibers experience large deformations during cardiac cycles. The fact that the elastin fibers and collagen were associated with the subendocardial Purkinje fibers (Figs. 7 and 10A), the branch point from the subendocardial Purkinje fibers (Fig. 10B), and the intramural Purkinje fibers (Fig. 10C) indicates the need for future studies on the detailed structure/composition of the Purkinje fiber ECM. Filling this knowledge gap is not only important to

understand Purkinje fiber anatomy, but also critical in gauging the ECM composition, amounts, and structural characteristics that need to be incorporated into Purkinje fiber tissue engineering and regeneration.

Restoring functional heart conduction pathways is always the dream of clinicians and bioengineers. Conductive biomaterials, including graphene, carbon nanotube, gold-based nanomaterials, and conductive polymers such as polyaniline and polypyrrole, have been investigated as a component in cardiac tissue engineering, showing potentials and certain material-specific limitations [61,62]. Most recently, Tracy et al. reported an effort to reprogram human adipogenic mesenchymal stem cells (hADMSCs) to form Purkinje cells and bioprint those cells into the Purkinje network by using Pluronic acid as the sacrificial material and type I collagen as the structural material [63]. Tracy et al. also reported that the bioprinted Purkinje networks were able to form continuous syncytium, express gap junction protein Connexin 40, and exhibit membrane potential changes when subjected to electric stimulation.

#### 4.4. Implications and applications in tissue engineering and 3D printing of bioactive materials

Our findings on cardiac elastin have many implications and potential applications to facilitate cardiac tissue engineering and bioactive

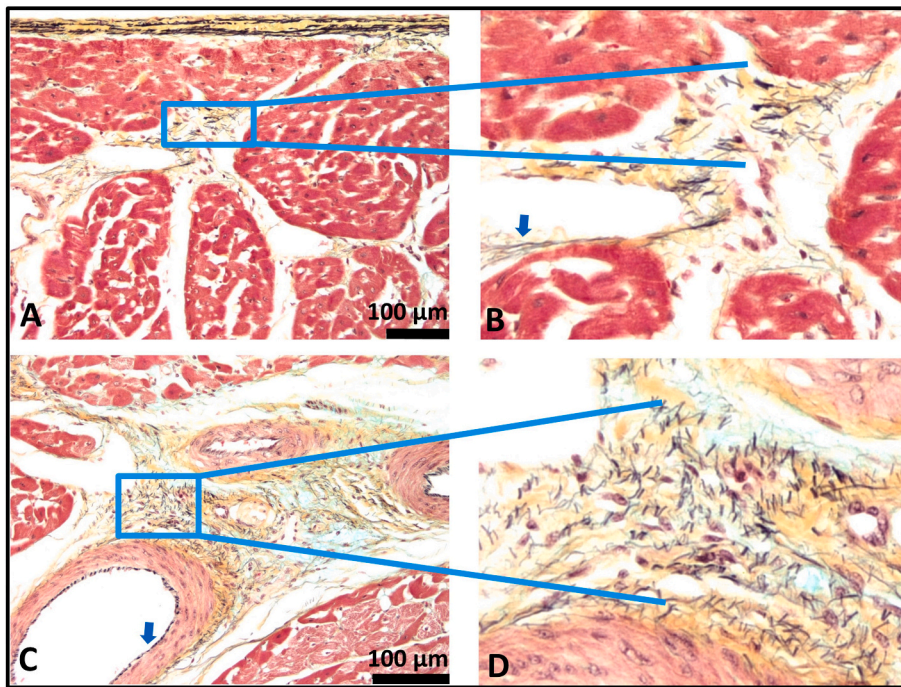


**Fig. 9.** Histological images of the LV myocardium cross-sections of the native porcine hearts, which featured blood vessels and elastin associated with blood vessels. The vascular elastin was observed in the walls of the blood vessels, especially in the intima and media layers (Arrows in B,C). In the collagen network that meshed the blood vessels to the surrounding myocardium, abundant interstitial elastin fibers existed, and this part of interstitial elastin fibers was more associated with the anatomical anchoring of the cardiac vasculature (rectangular boxes in A,C, and zoomed-in details of those boxes as in B,D). Movat's pentachrome staining: Collagen in yellow, elastin fibers in black, and cardiac muscles in red. Scale bar = 100  $\mu\text{m}$ .

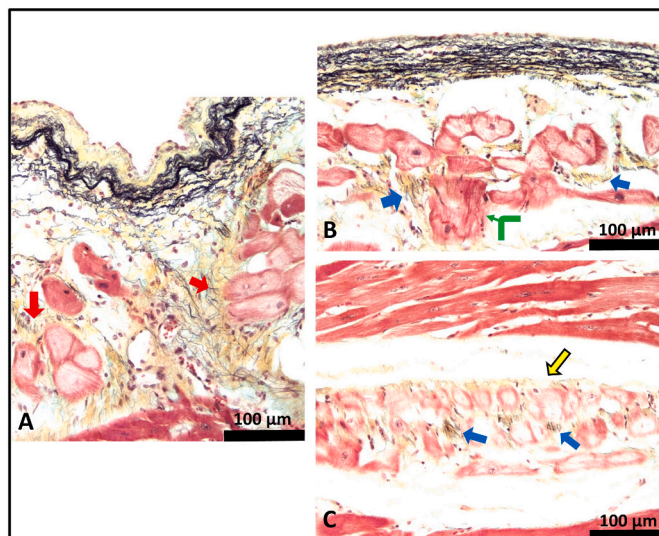


**Fig. 10.** Histological images of the LV endocardial cross-sections (A) and (B) and LV myocardium cross-section (C) of the native porcine hearts showed that fine elastin fibers, along with collagen network, closely associated with the Purkinje cells, implying that this ECM association could be essential in organizing cardiac Purkinje cells into “fibrous” and “branching” morphologies. We noticed that the fine elastin fibers, meshing with collagen fibers, morphologically wrapped around groups of Purkinje cells (cell groups in cross-sectional view) (red arrows in A). Moreover, the fine elastin fiber arrays, which had local alignment, were also frequently observed scattering in-between the Purkinje cells, and those elastin fiber arrays always associating with yellow-stained collagen (blue arrows in B,C). We also captured the elastin fibers and collagen that were associated with subendocardial Purkinje fibers (A,B), the elastin fibers and collagen associated with the branch point from subendocardial Purkinje fibers (green arrow in B shows where T-shape branching happens), and the elastin fibers and collagen associated with the intramural Purkinje fibers (yellow arrow in C). Movat's pentachrome staining: Collagen in yellow, elastin fibers in black, cardiac muscles in red, and the Purkinje fibers in pale pink. Scale bar = 100  $\mu\text{m}$ .

material design. For instance, cardiac patch design can target the mimicking of the epicardial prestraining protective mechanism [39]. Serving as a natural protective interface, the elastin-rich, prestrained epicardial layer provides additional resistance against ventricular diastolic expansion and ventricular wall protection by reducing myocardial stress, as well as assisting efficient energy storage and release during heart diastolic and systolic phases [39]. Moreover, the unique biomechanical properties and microstructure of the native epicardial layer deem it an option as a potential tissue-derived scaffolds for cardiac patch application after decellularization. For cardiac tissue engineering, Gonzalez de Torre et al. reviewed the advances and importance of using elastin-based materials for cardiac tissue regeneration applications [64]. Elastin-based scaffolds were found suitable as cardiac therapeutics by not only providing mechanical properties and guiding cardiomyocyte adhesion and proliferation, but also triggering angiogenesis to functionalize the final product [64–67].

With the Purkinje fiber ECM morphology demonstrated by our histological images, one could envision that future efforts on tissue engineered or bioprinted Purkinje fibers/network could benefit by including both the collagen and elastin components as structural supporting materials. As a nature-optimized combination, ECM network meshed by collagen fibers and elastin fibers can simultaneously provide extensibility, mechanical strength, and over-stretch protection, while minimizing energy dissipation during dynamic loading. All those qualities are much needed for the engineered Purkinje fibers/network when they are eventually integrated into ventricular wall where they will have to experience cyclic large deformation *in vivo*.”

## 5. Conclusion

In this study, we investigated the spatial distribution and microstructural morphologies of cardiac elastin in porcine left ventricle. A summary of our major findings is listed as follows.

- (1) Using LSCM, we obtained a detailed mapping of the epicardial elastin network on the left ventricle. We showed that the epicardial elastin network had location-dependency, i.e., having various network patterns at different anatomic locations, as

shown by the 3D images from the anterior base, lateral base, posterior base, anterior middle, lateral middle, posterior middle, and apex. Besides the location-dependency, epicardial elastin network also showed depth-dependency, with fiber alignment and microstructure varying from the surface to the deeper layer. Moreover, the overall epicardial elastin fiber orientation showed certain correlation with the helical heart muscle fiber architecture revealed by DT-MRI.

- (2) Histological analysis demonstrated that, when compared to the epicardial layer, the endocardial layer was thicker and has a higher elastin-collagen ratio and denser elastin fiber network; moreover, endocardial elastin fibers were finer and more wavy than the epicardial elastin fibers. Those microstructural variations might be related with the different interface mechanics associated with the endocardial surface and epicardial surface.
- (3) In the myocardium, we demonstrated that the myocardial interstitial elastin fibers co-existed with the perimysial collagen to bind and connect the cardiomyocyte bundles. Some interstitial elastin fibers showed locally-aligned, hinge-like structures to connect the adjacent cardiomyocyte bundles. This combination is an optimal nature design, in which the collagen fibers provide mechanical strength during diastolic phase and the elastin fibers facilitate recoiling during systolic phase.
- (4) Lastly, we showed that fine elastin fibers, along with collagen network, were closely associated with the Purkinje cells, hinting that this ECM association could be essential in organizing cardiac Purkinje cells into “fibrous” and “branching” morphologies, possibly also serving as a protective feature when the electrically conductive Purkinje fibers experience large deformations during diastolic and systolic phases.
- (5) Our findings on cardiac elastin indicate potential applications that can facilitate cardiac tissue engineering and bioactive material design. As examples, cardiac patch tissue engineering can target the mimicking of the epicardial prestraining protective mechanism, as well as use acellular epicardial layer as patch scaffolds; future efforts on tissue engineered or bioprinted Purkinje fibers/network could also be benefited by including both the collagen and elastin components as structural supporting materials.

Our future study will include human heart model to further establish translational basis for cardiac elastin research. In short, our study revealed novel microstructural characteristics of cardiac elastin and established a structural foundation for future in-depth biomechanical investigations such as age-dependency and diseased alterations, as well as biomimicking of this long overlooked cardiac ECM component.

#### CRedit authorship contribution statement

**Xiaodan Shi:** Conceptualization, Methodology, Investigation, Writing – original draft, Writing – review & editing. **Song Zhang:** Conceptualization, Investigation, Visualization. **Yue Liu:** Investigation. **Bryn Brazile:** Investigation. **Jim Cooley:** Investigation, Methodology. **J. Ryan Butler:** Conceptualization, Investigation. **Sara R. McMahan:** Investigation. **Karla L. Perez:** Investigation. **Jiazhu Xu:** Investigation. **Timothy Eastep:** Investigation. **Kytai T. Nguyen:** Investigation, Writing – review & editing. **Pietro Bajona:** Investigation, Writing – review & editing. **Matthias Peltz:** Investigation, Writing – review & editing. **Huajian Gao:** Conceptualization, Writing – review & editing. **Yi Hong:** Investigation, Writing – review & editing. **Jun Liao:** Conceptualization, Methodology, Investigation, Writing – original draft, Writing – review & editing, Funding acquisition.

#### Declaration of competing interest

The authors declare that they have no known competing financial

interests or personal relationships that could have appeared to influence the work reported in this paper.

#### Acknowledgements

The authors would appreciate the following funding support: R01EB022018, R15HL140503, and T32 HL134613 from NIH, and UT STARS. The authors would also like to thank the technique support from Ms. Amanda Lawrence and Ms. I-Wei Chu in LSCM.

#### References

- [1] E.J. Benjamin, P. Muntner, A. Alonso, M.S. Bittencourt, C.W. Callaway, A. P. Carson, A.M. Chamberlain, A.R. Chang, S. Cheng, S.R. Das, F.N. Delling, L. Djousse, M.S.V. Elkind, J.F. Ferguson, M. Fornage, L.C. Jordan, S.S. Khan, B. M. Kissela, K.L. Knutson, T.W. Kwan, D.T. Lackland, T.T. Lewis, J.H. Lichtman, C. T. Longenecker, M.S. Loop, P.L. Lutsey, S.S. Martin, K. Matsushita, A.E. Moran, M. E. Mussolino, M. O’Flaherty, A. Pandey, A.M. Perak, W.D. Rosamond, G.A. Roth, U. K.A. Sampson, G.M. Satou, E.B. Schroeder, S.H. Shah, N.L. Spartano, A. Stokes, D. L. Tirschwell, C.W. Tsao, M.P. Turakhia, L.B. VanWagner, J.T. Wilkins, S.S. Wong, S.S. Virani, E. American Heart Association Council on, C. Prevention Statistics, S. Stroke Statistics, Heart disease and stroke statistics-2019 update: a report from the American heart association, *Circulation* 139 (10) (2019) e56–e528.
- [2] W. Raab, The nonvascular metabolic myocardial vulnerability factor in “coronary heart disease”. *Fundamentals of pathogenesis, treatment, and prevention, Am. Heart J.* 66 (1963) 685–706.
- [3] G. Baroldi, Coronary heart disease: significance of the morphologic lesions, *Am. Heart J.* 85 (1) (1973) 1–5.
- [4] G. Baroldi, Acute coronary occlusion as a cause of myocardial infarct and sudden coronary heart death, *Am. J. Cardiol.* 16 (6) (1965) 859–880.
- [5] L.R. Erhardt, G. Unge, G. Boman, Formation of coronary arterial thrombi in relation to onset of necrosis in acute myocardial infarction in man. A clinical and autoradiographic study, *Am. Heart J.* 91 (5) (1976) 592–598.
- [6] D.D. Reichenbach, N.S. Moss, Myocardial cell necrosis and sudden death in humans, *Circulation* 52 (6 Suppl) (1975) III60–I62.
- [7] M.D. Silver, T.W. Anderson, A.A. Vand Dreumel, R.E. Hutson, Letter: nutritional muscular dystrophy and human myocardial infarction, *Lancet* 2 (7834) (1973) 912–913.
- [8] J. Narula, N. Haider, R. Virmani, T.G. DiSalvo, F.D. Kolodgie, R.J. Hajjar, U. Schmidt, M.J. Semigran, G.W. Dec, B.A. Khaw, Apoptosis in myocytes in end-stage heart failure, *N. Engl. J. Med.* 335 (16) (1996) 1182–1189.
- [9] E.D. Robin, Special report: dysoxia. Abnormal tissue oxygen utilization, *Arch. Intern. Med.* 137 (7) (1977) 905–910.
- [10] J.P. Cleutjens, W.M. Blanksteijn, M.J. Daemen, J.F. Smits, The infarcted myocardium: simply dead tissue, or a lively target for therapeutic interventions, *Cardiovasc. Res.* 44 (2) (1999) 232–241.
- [11] T. De Celle, J.P. Cleutjens, W.M. Blanksteijn, J.J. Debets, J.F. Smits, B.J. Janssen, Long-term structural and functional consequences of cardiac ischaemia-reperfusion injury in vivo in mice, *Exp. Physiol.* 89 (5) (2004) 605–615.
- [12] A.R. Gaby, Nutritional treatments for acute myocardial infarction, *Alternative Med. Rev. : J. Clin. Therapeutic* 15 (2) (2010) 113–123.
- [13] J.R. Venugopal, M.P. Prabhakaran, S. Mukherjee, R. Ravichandran, K. Dan, S. Ramakrishna, Biomaterial strategies for alleviation of myocardial infarction, *J. R. Soc. Interface* 9 (66) (2012) 1–19.
- [14] J.D. Dowell, L.J. Field, K.B. Pasumarthi, Cell cycle regulation to repair the infarcted myocardium, *Heart Fail. Rev.* 8 (3) (2003) 293–303.
- [15] K.B. Pasumarthi, L.J. Field, Cardiomyocyte cell cycle regulation, *Circ. Res.* 90 (10) (2002) 1044–1054.
- [16] J.T. McMahon, N.B. Ratliff, Regeneration of adult human myocardium after acute heart transplant rejection, *J. Heart Transplant.* 9 (5) (1990) 554–567.
- [17] R. Sharma, R. Raghur, Stem cell therapy: a hope for dying hearts, *Stem Cell. Dev.* 16 (4) (2007) 517–536.
- [18] R.W. Grauss, E.M. Winter, J. van Tuyn, D.A. Pijnappels, R.V. Steijn, B. Hogers, R. J. van der Geest, A.A. de Vries, P. Teendijk, A. van der Laarse, A.C. Gittenberger-de Groot, M.J. Schalij, D.E. Atsma, Mesenchymal stem cells from ischemic heart disease patients improve left ventricular function after acute myocardial infarction, *Am. J. Physiol. Heart Circ. Physiol.* 293 (4) (2007) H2438–H2447.
- [19] B.E. Strauer, R. Kornowski, Stem cell therapy in perspective, *Circulation* 107 (7) (2003) 929–934.
- [20] R.Y. Kannan, H.J. Salacinski, K. Sales, P. Butler, A.M. Seifalian, The roles of tissue engineering and vascularisation in the development of micro-vascular networks: a review, *Biomaterials* 26 (14) (2005) 1857–1875.
- [21] C. Williams, L.D. Black III, *The Role of Extracellular Matrix in Cardiac Development*, Biomaterials for Cardiac Regeneration, Springer, 2015, pp. 1–35.
- [22] G.M. Fomovsky, S. Thomopoulos, J.W. Holmes, Contribution of extracellular matrix to the mechanical properties of the heart, *J. Mol. Cell. Cardiol.* 48 (3) (2010) 490–496.
- [23] T. Borg, J. Caulfield, *The Collagen Matrix of the Heart*, Federation proceedings, 1981, pp. 2037–2041.
- [24] M.A. Sussman, A. McCulloch, T.K. Borg, Dance band on the titanic biomechanical signaling in cardiac hypertrophy, *Circ. Res.* 91 (10) (2002) 888–898.

- [25] B. Wang, M.E. Tedder, C.E. Perez, G. Wang, A.L. de Jongh Curry, F. To, S.H. Elder, L.N. Williams, D.T. Simionescu, J. Liao, Structural and biomechanical characterizations of porcine myocardial extracellular matrix, *J. Mater. Sci. Mater. Med.* 23 (8) (2012) 1835–1847.
- [26] P.D. Jöbbsis, H. Ashikaga, H. Wen, E.C. Rothstein, K.A. Horvath, E.R. McVeigh, R. S. Balaban, The visceral pericardium: macromolecular structure and contribution to passive mechanical properties of the left ventricle, *Am. J. Physiol. Heart Circ. Physiol.* 293 (6) (2007) H3379–H3387.
- [27] T. Chowdhury, W. Reardon, Elastin mutation and cardiac disease, *Pediatr. Cardiol.* 20 (2) (1999) 103–107.
- [28] M. Perou, Congenital supraaortic stenosis. A morphological study with attempt at classification, *Arch. Pathol.* 71 (1961) 453.
- [29] W. O'connor, J. Davis Jr., R. Geissler, C. Cottrill, J. Noonan, E. Todd, Supraaortic aortic stenosis. Clinical and pathologic observations in six patients, *Arch. Pathol. Lab Med.* 109 (2) (1985) 179–185.
- [30] M. Bloksgaard, T.M. Leurgans, I. Nissen, P.S. Jensen, M.L. Hansen, J.R. Brewer, L. A. Bagatolli, N. Marcussen, A. Irmukhamedov, L.M. Rasmussen, Elastin organization in pig and cardiovascular disease patients' pericardial resistance arteries, *J. Vasc. Res.* 52 (1) (2015) 1–11.
- [31] T. Mizuno, T.M. Yau, R.D. Weisel, C.G. Kiani, R.-K. Li, Elastin stabilizes an infarct and preserves ventricular function, *Circulation* 112 (9 suppl) (2005) I–81.
- [32] S.H. Li, Z. Sun, L. Guo, M. Han, M.F. Wood, N. Ghosh, I. Alex Vitkin, R.D. Weisel, R. K. Li, Elastin overexpression by cell-based gene therapy preserves matrix and prevents cardiac dilation, *J. Cell Mol. Med.* 16 (10) (2012) 2429–2439.
- [33] V.S. Mujumdar, S.C. Tyagi, Temporal regulation of extracellular matrix components in transition from compensatory hypertrophy to decompensatory heart failure, *J. Hypertens.* 17 (2) (1999) 261–270.
- [34] T.E. Raya, R.G. Gay, L. Lancaster, M. Aguirre, C. Moffett, S. Goldman, Serial changes in left ventricular relaxation and chamber stiffness after large myocardial infarction in rats, *Circulation* 77 (6) (1988) 1424–1431.
- [35] K.B. Gupta, M.B. Ratcliffe, M.A. Fallert, L.H. Edmunds Jr., D.K. Bogen, Changes in passive mechanical stiffness of myocardial tissue with aneurysm formation, *Circulation* 89 (5) (1994) 2315–2326.
- [36] S. Sato, M. Ashraf, R.W. Millard, H. Fujiwara, A. Schwartz, Connective tissue changes in early ischemia of porcine myocardium: an ultrastructural study, *J. Mol. Cell. Cardiol.* 15 (4) (1983) 261–275.
- [37] B.C. Henderson, U. Sen, C. Reynolds, K.S. Moshal, A. Ovechkin, N. Tyagi, G. K. Kartha, W.E. Rodriguez, S.C. Tyagi, Reversal of systemic hypertension-associated cardiac remodeling in chronic pressure overload myocardium by ciglitazone, *Int. J. Biol. Sci.* 3 (6) (2007) 385–392.
- [38] X.W. Cheng, K. Obata, M. Kuzuya, H. Izawa, K. Nakamura, E. Asai, T. Nagasaka, M. Saka, T. Kimata, A. Noda, K. Nagata, H. Jin, G.P. Shi, A. Iguchi, T. Murohara, M. Yokota, Elastolytic cathepsin induction/activation system exists in myocardium and is upregulated in hypertensive heart failure, *Hypertension* 48 (5) (2006) 979–987.
- [39] X. Shi, Y. Liu, K.M. Copeland, S.R. McMahan, S. Zhang, J.R. Butler, Y. Hong, M. Cho, P. Bajona, H. Gao, J. Liao, Epicardial prestrained confinement and residual stresses: a newly observed heart ventricle confinement interface, *J. R. Soc. Interface* 16 (152) (2019) 20190028.
- [40] C. Farquharson, S.P. Robins, The distribution of elastin in developing and adult rat organs using immunocytochemical techniques, *J. Anat.* 165 (1989) 225.
- [41] G. Hasenfuss, Animal models of human cardiovascular disease, heart failure and hypertrophy, *Cardiovasc. Res.* 39 (1) (1998) 60–76.
- [42] S.J. Crick, M.N. Sheppard, S.Y. Ho, L. Gebstein, R.H. Anderson, Anatomy of the pig heart: comparisons with normal human cardiac structure, *J. Anat.* 193 (Pt 1) (1998) 105–119.
- [43] J.A. Ambrose, Myocardial ischemia and infarction, *J. Am. Coll. Cardiol.* 47 (11 Suppl) (2006) D13–D17.
- [44] B. Wang, A. Borazjani, M. Tahai, A.L. de Jongh Curry, D.T. Simionescu, J. Guan, F. To, S.H. Elder, J. Liao, Fabrication of cardiac patch with decellularized porcine myocardial scaffold and bone marrow mononuclear cells, *J. Biomed. Mater. Res.* 94 (4) (2010) 1100–1110.
- [45] Y.-C. Liu, A.-S. Chiang, High-resolution confocal imaging and three-dimensional rendering, *Methods* 30 (1) (2003) 86–93.
- [46] M. Werner, A. Chott, A. Fabiano, H. Battifora, Effect of formalin tissue fixation and processing on immunohistochemistry, *Am. J. Surg. Pathol.* 24 (7) (2000) 1016–1019.
- [47] B.C. Weed, A. Borazjani, S.S. Patnaik, R. Prabhu, M. Horstemeyer, P.L. Ryan, T. Franz, L.N. Williams, J. Liao, Stress state and strain rate dependence of the human placenta, *Ann. Biomed. Eng.* 40 (10) (2012) 2255–2265.
- [48] P.S. Clifford, S.R. Ella, A.J. Stupica, Z. Nourian, M. Li, L.A. Martinez-Lemus, K. A. Dora, Y. Yang, M.J. Davis, U. Pohl, Spatial distribution and mechanical function of elastin in resistance arteries A role in bearing longitudinal stress, *Arterioscler. Thromb. Vasc. Biol.* 31 (12) (2011) 2889–2896.
- [49] W.R. Zipfel, R.M. Williams, R. Christie, A.Y. Nikitin, B.T. Hyman, W.W. Webb, Live tissue intrinsic emission microscopy using multiphoton-excited native fluorescence and second harmonic generation, *Proc. Natl. Acad. Sci. Unit. States Am.* 100 (12) (2003) 7075–7080.
- [50] T.F. Robinson, L. Cohen-Gould, S.M. Factor, Skeletal framework of mammalian heart muscle. Arrangement of inter- and pericardial connective tissue structures, *Lab. Invest.* 49 (4) (1983) 482–498.
- [51] T.F. Robinson, L. Cohen-Gould, S.M. Factor, M. Eghbali, O.O. Blumenfeld, Structure and function of connective tissue in cardiac muscle: collagen types I and III in endomyocardial struts and pericellular fibers, *Scanning Microsc.* 2 (2) (1988) 1005–1015.
- [52] V. Garcia-Bustos, R. Sebastian, M. Izquierdo, P. Molina, F.J. Chorro, A. Ruiz-Sauri, A quantitative structural and morphometric analysis of the Purkinje network and the Purkinje-myocardial junctions in pig hearts, *J. Anat.* 230 (5) (2017) 664–678.
- [53] R.S. Stephenson, A. Atkinson, P. Kottas, F. Perde, F. Jafarzadeh, M. Bateman, P. A. Iaizzo, J. Zhao, H. Zhang, R.H. Anderson, J.C. Jarvis, H. Dobrzynski, High resolution 3-Dimensional imaging of the human cardiac conduction system from microanatomy to mathematical modeling, *Sci. Rep.* 7 (1) (2017) 7188.
- [54] A.J. Atkinson, S.J. Logantha, G. Hao, J. Yanni, O. Fedorenko, A. Sinha, S.H. Gilbert, A.P. Benson, D.L. Buckley, R.H. Anderson, M.R. Boyett, H. Dobrzynski, Functional, anatomical, and molecular investigation of the cardiac conduction system and arrhythmogenic atrioventricular ring tissue in the rat heart, *J. Am. Heart Assoc.* 2 (6) (2013), e000246.
- [55] D.J. Pennisi, S. Rentschler, R.G. Gourdie, G.I. Fishman, T. Mikawa, Induction and patterning of the cardiac conduction system, *Int. J. Dev. Biol.* 46 (6) (2002) 765–775.
- [56] S.M. Arribas, C.J. Daly, M.C. González, J.C. McGrath, Imaging the vascular wall using confocal microscopy, *J. Physiol.* 584 (1) (2007) 5–9.
- [57] C.J. Gerson, S. Goldstein, A.E. Heacox, Retained structural integrity of collagen and elastin within cryopreserved human heart valve tissue as detected by two-photon laser scanning confocal microscopy, *Cryobiology* 59 (2) (2009) 171–179.
- [58] B. Mills, A.R. Akram, E. Scholefield, M. Bradley, K. Dhaliwal, Optical screening of novel bacteria-specific probes on Ex vivo human lung tissue by confocal laser endomicroscopy, *JoVE* 129 (2017).
- [59] S. Zhang, J.A. Crow, X. Yang, J. Chen, A. Borazjani, K.B. Mullins, W. Chen, R. C. Cooper, R.M. McLaughlin, J. Liao, The correlation of 3D DT-MRI fiber disruption with structural and mechanical degeneration in porcine myocardium, *Ann. Biomed. Eng.* 38 (10) (2010) 3084–3095.
- [60] T. Mizuno, D.A. Mickle, C.G. Kiani, R.-K. Li, Overexpression of elastin fragments in infarcted myocardium attenuates scar expansion and heart dysfunction, *Am. J. Physiol. Heart Circ. Physiol.* 288 (6) (2005) H2819–H2827.
- [61] A. Mousavi, S. Vahdat, N. Baheiraei, M. Razavi, M.H. Norahan, H. Baharvand, Multifunctional conductive biomaterials as promising platforms for cardiac tissue engineering, *ACS Biomater. Sci. Eng.* 7 (1) (2021) 55–82.
- [62] R. Dong, P.X. Ma, B. Guo, Conductive biomaterials for muscle tissue engineering, *Biomaterials* 229 (2020) 119584.
- [63] E.P. Tracy, B.C. Gettler, J.S. Zakhari, R.J. Schwartz, S.K. Williams, R.K. Birla, 3D bioprinting the cardiac Purkinje system using human adipogenic mesenchymal stem cell derived Purkinje cells, *Cardiovascular Eng. Technol.* 11 (5) (2020) 587–604.
- [64] I. Gonzalez de Torre, M. Alonso, J.C. Rodriguez-Cabello, Elastin-based materials: promising candidates for cardiac tissue regeneration, *Front. Bioeng. Biotechnol.* 8 (2020) 657.
- [65] N. Annabi, K. Tsang, S.M. Mithieux, M. Nikkhah, A. Ameri, A. Khademhosseini, A. S. Weiss, Highly elastic micropatterned hydrogel for engineering functional cardiac tissue, *Adv. Funct. Mater.* 23 (39) (2013).
- [66] A. Robinet, A. Fahem, J.H. Cauchard, E. Huet, L. Vincent, S. Lorimier, F. Antonicelli, C. Soria, M. Crepin, W. Hornebeck, G. Bellon, Elastin-derived peptides enhance angiogenesis by promoting endothelial cell migration and tubulogenesis through upregulation of MT1-MMP, *J. Cell Sci.* 118 (Pt 2) (2005) 343–356.
- [67] C.J. Reddel, D. Cultrone, J. Rnjak-Kovacina, A.S. Weiss, J.K. Burgess, Tropoelastin modulates TGF-beta1-induced expression of VEGF and CTGF in airway smooth muscle cells, *Matrix Biol.* 32 (7–8) (2013) 407–413.